ChemComm

COMMUNICATION

View Article Online
View Journal

Cite this: DOI: 10.1039/c5cc09158f

Received 4th November 2015,
Accepted 14th December 2015

DOI: 10.1039/c5cc09158f

www.rsc.org/chemcomm

The fabrication of $BiOCl_xBr_{1-x}$/alumina composite films with highly exposed {001} facets and their superior photocatalytic activities†

Anirban Dandapat,* Hani Gnayem and Yoel Sasson*

We report the fabrication of thin films of bismuth oxyhalide solid solution with highly exposed {001} facets with the help of cetyltrimethylammonium bromide and aluminium oxyhydroxide. These {001} facet exposed films showed enhanced photocatalytic activities compared to those of randomly oriented facets.

Crystal facet engineering of semiconductor materials is of emergent interest since different crystal facets have different geometric and electronic structures, exhibiting intrinsic physical and chemical properties related to the crystallographic orientation.[1–6] Synthesis of materials with any specific facet has always been a great challenge.

Bismuth oxyhalides (BiOXs, X = F, Cl, Br, I), a new family of promising semiconductor photocatalysts, have been attracting much interest because of their extraordinary photocatalytic activities under solar light irradiation.[7–11] Several approaches have been adopted for further enhancing the photocatalytic activities of BiOXs, including alloying, elemental doping, metal (or semiconductor) coupling, and facet oriented fabrication.[1,12,13] As one of the potential methods for better photocatalytic performances, the effect of different facets on their activity has been studied widely over the past few years.[1,14–18] BiOX with exposed {001} facets exhibited better visible light driven photocatalysis for various chemical and oxidation reactions as well as bacterial inactivation.[14–16,19,20] Theoretical calculations also suggested better activity of {001} facets over {110} facets for BiOX.[21] Recently another approach has been adopted by preparing solid solution of different oxyhalides to create heterojunctions with interlaced band structures that provide better visible-light response and efficient separation of the electron–hole pairs, and thus exhibited enhanced photocatalytic activities.[7,22,23] Additionally, for practical applications, the development of the materials in the form of coatings or thin films is highly desirable.[24,25] It would be highly beneficial if it becomes possible to achieve all these benefits in a single approach. To the best of our knowledge, we are first to report the fabrication of thin films of bismuth oxyhalide solid solution with highly exposed {001} facets. These {001} facet exposed films showed better photocatalytic activities compared to the randomly oriented facets.

$BiOCl_xBr_{1-x}$ microspheres were first synthesized in a simple wet chemical procedure at room temperature.[7] All the XRD peaks of the as-synthesized product ($BiOCl_xBr_{1-x}$-AS) can be indexed to the tetrahedral $BiOCl_xBr_{1-x}$ (JCPDS # 00-063-0068) crystals. The composition of the solid solution was estimated to be $BiOCl_{0.8}Br_{0.2}$, which is calculated from the lattice parameters of pure BiOCl (JCPDS # 01-085-0861) and BiOBr (JCPDS # 00-009-0393). Then $BiOCl_xBr_{1-x}$-AS was ultrasonicated for 5 minutes with CTAB solutions followed by mixing with aluminium oxyhydroxide sol and re-ultrasonicated for further 5 minutes. Then a stable highly viscous sol was formed. The coatings on glass substrates were prepared by a simple smearing technique with the composite sol. The films were dried and heat-treated at 350 °C with a slow heating rate (1° min^{-1}). A stoichiometric amount of CTAB was optimized to achieve the highest orientation of {001} facets (ESI;† Fig. S1). Interestingly, XRD patterns (Fig. 1) of the optimized film revealed that the peak corresponding to (001) has a very high intensity and its parallel plane (002) also has significant intensity, however other planes were almost vanished in contrast to the case of $BiOCl_xBr_{1-x}$-AS and calcined $BiOCl_{0.8}Br_{0.2}$ powders ($BiOCl_xBr_{1-x}$ – 350 °C). It implies that the $BiOCl_{0.8}Br_{0.2}$/alumina film contains very high percentage of {001} facets. The I_{001}/I_{110} value of $BiOCl_{0.8}Br_{0.2}$/alumina (I_{001}/I_{110} = 15.2) is much higher than those of $BiOCl_xBr_{1-x}$-AS (I_{001}/I_{110} = 0.07) and $BiOCl_xBr_{1-x}$ – 350 °C (I_{001}/I_{110} = 0.18), suggesting that the percentage of {001} facets in $BiOCl_{0.8}Br_{0.2}$/alumina films is much higher than that in as-prepared and 350 °C calcinated $BiOCl_{0.8}Br_{0.2}$ powders. On the other hand, XRD peaks (ESI;† Fig. S2) for aluminium oxyhydroxide were absent in the composite films suggesting the possible transformation of aluminium oxyhydroxide into aluminium oxide during the calcinations.

SEM characterization of the films was given in Fig. 2. Both the top and the cross-sectional view of the films reveal that the

Casali Center of Applied Chemistry, Institute of Chemistry, The Hebrew University of Jerusalem, Jerusalem 91904, Israel. E-mail: anirban.dandapat@mail.huji.ac.il, ysasson@huji.ac.il

† Electronic supplementary information (ESI) available. See DOI: 10.1039/c5cc09158f

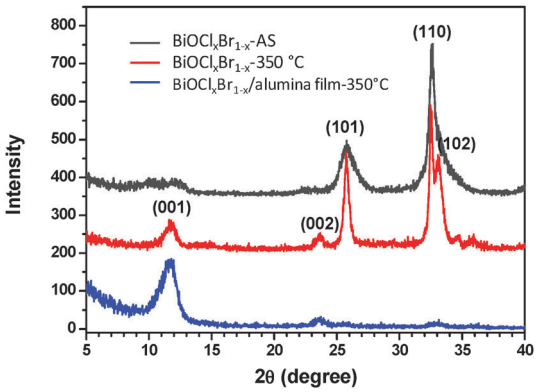

Fig. 1 XRD patterns of the BiOCl$_x$Br$_{1-x}$ powders and BiOCl$_x$Br$_{1-x}$/alumina composite film.

ultrasonic treatment in the presence of CTAB and AlOOH, followed by their calcinations leads to the rupture of the microspheres into individual petals and assemblies of these petals with the help of alumina as glue finally to form stable coatings. We performed SEM-EDX line scanning analyses of the composite film (ESI;† Fig. S3a) deposited on glass substrates to check the concentration profile of BiOX along the depth of the film. The EDX profile of Al, Bi, Cl, Br (ESI;† Fig. S3b) confirms their uniform distribution along the film thickness (~2 μm). This result indicates that BiOX microspheres are broken into individual plates and formed a uniform composite to develop

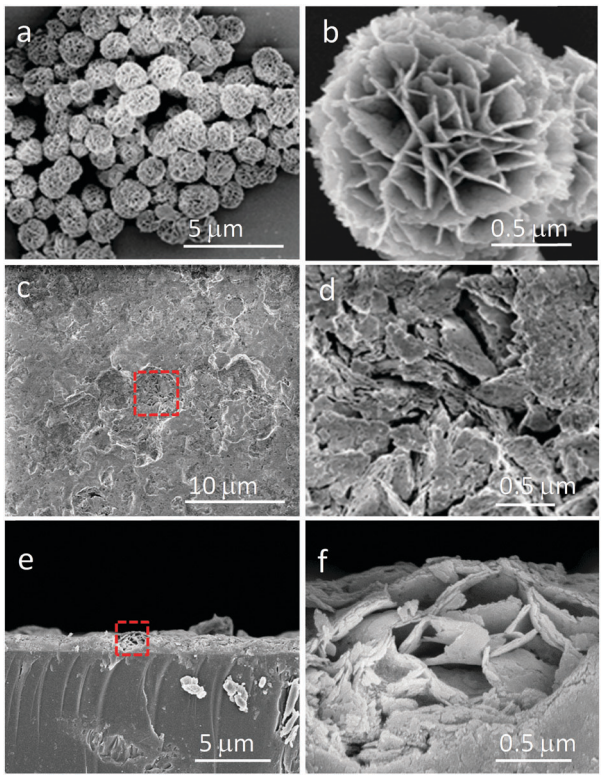

Fig. 2 SEM images of the microstructures: (a and b) BiOCl$_x$Br$_{1-x}$-AS powders and (c–f) BiOCl$_x$Br$_{1-x}$/alumina composite films. Both the top (c and d) and cross-sectional (e and f) view of the films were shown.

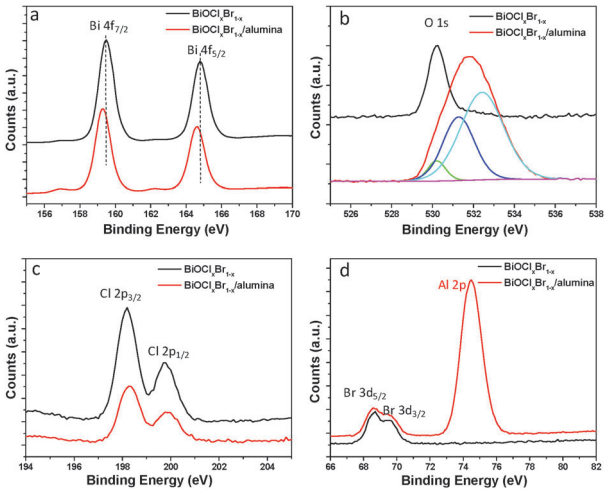

Fig. 3 High resolution XPS spectra of the BiOCl$_x$Br$_{1-x}$ and BiOCl$_x$Br$_{1-x}$/alumina composite films: (a) the Bi 4f region, (b) the O 1s region, (c) the Cl 2p region, (d) Br 3d and Al 2p regions.

the films. The profiles of oxygen and Si (from substrate) are also shown along the film thickness (ESI;† Fig. S3b). The composite films have a very strong adhesion with the glass substrate which ensures the use of these coatings for practical applications.

The diffuse reflectance spectrum (Fig. S4; ESI†) of the composite film was collected to estimate the band gap (2.94 eV). Surface area of the composite film was estimated to be 70.6 m^2 g^{-1}. FTIR spectra (Fig. S5; ESI†) of the composite films calcined at 350 °C do not have the characteristic peaks for AlOOH, rather some broad peaks arrived near 922, 830, 720, and 587 cm^{-1} indicating the formation of the Al_2O_3 phase[26] along with the presence of a peak around 525 cm^{-1} for the Bi–O bond.[27] The surface chemical compositions and oxidation states of the BiOCl$_{0.8}$Br$_{0.2}$/alumina composite films were investigated by X-ray photoelectron spectroscopy (XPS). XPS analysis of BiOCl$_{0.8}$Br$_{0.2}$ microspheres was also shown for comparative studies and the characteristic peaks for Bi 4f, O 1s, Cl 2p and Br 3d were identified as shown in Fig. 3. However, Bi 4f peaks in the BiOCl$_{0.8}$Br$_{0.2}$/alumina composite displayed a slight shift as compared to the Bi 4f peak in the pure BiOCl$_{0.8}$Br$_{0.2}$ materials, suggesting the possible interaction between alumina and BiOCl$_{0.8}$Br$_{0.2}$. In pure BiOCl$_{0.8}$Br$_{0.2}$ powders, the O 1s peak at 530.2 eV was attributed to the oxygen in BiOCl$_{0.8}$Br$_{0.2}$ materials. Whereas, the composite film showed a broad peak for O 1s which comes from overlapping contributions of oxide ions (O^{2-}) of alumina and Bi–O moieties. XPS spectra of Cl 2p and Br 3d were almost similar for both BiOCl$_{0.8}$Br$_{0.2}$ powders and composite films. Additional Al 2p peaks of Al^{3+} appeared in the composite film due to the presence of alumina.[28,29]

A TEM study of the composite films was conducted and presented in Fig. 4. The high resolution TEM (HRTEM) image (Fig. 4a) of the nanoplates reveals a lattice spacing of 0.76 nm, matching well with (001) interplanar spacing. Again, the HRTEM images (Fig. 4c) viewed from the [001] zone axis clearly show two sets of lattice fringes with a lattice spacing of 0.275 nm, corresponding to those of the (110) and (1$\bar{1}$0) facets, those are right angle to each other. In addition, SAED patterns (Fig. 4e)

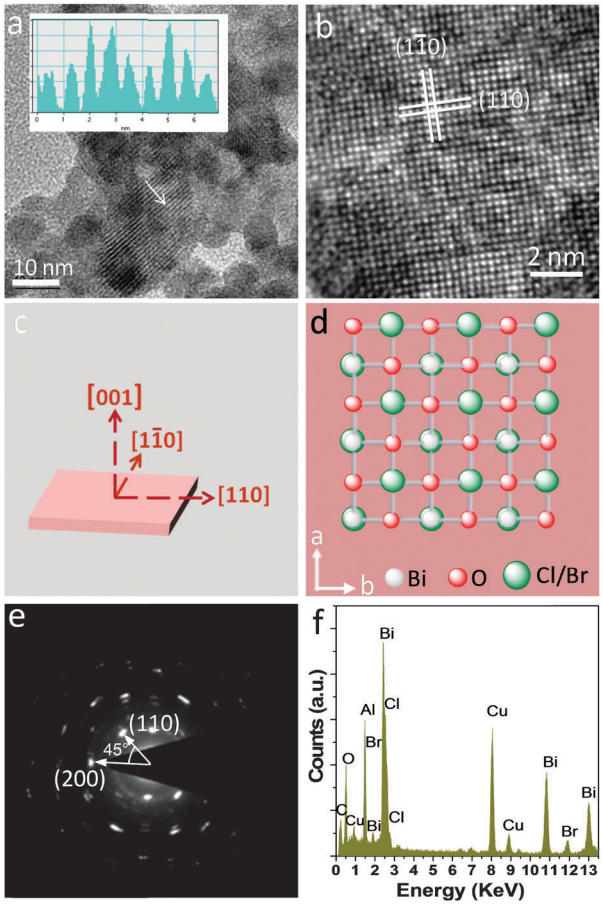

Fig. 4 TEM characterization of $BiOCl_xBr_{1-x}$/alumina composite films: (a and b) HRTEM images; Inset of Fig. 4(a) shows the profile of spacings between the lattice fringes along the white line; (c) schematic view and (d) atomic orientation of {001} facets; (e) SAED and (f) EDS patterns of the samples.

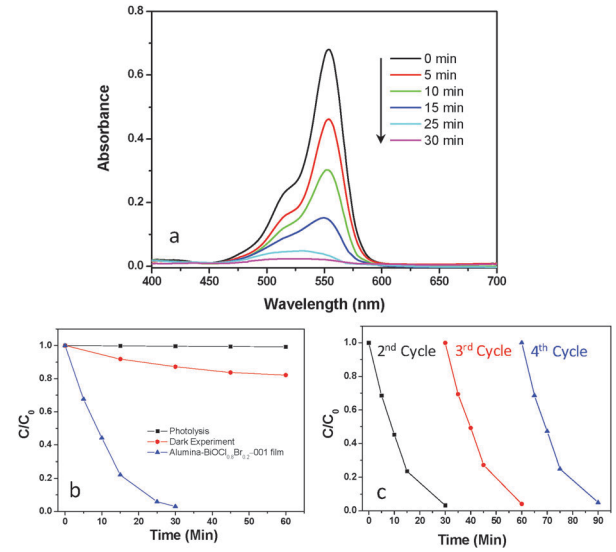

Fig. 5 Photocatalytic activities of the composite coatings towards RhB decomposition.

also showed a 90° angle between the (110) and (1$\bar{1}$0) planes. The angle of adjacent spots labeled as (110) and (200) planes is 45°. The set of diffraction spots can be indexed as the [001] zone axis of tetragonal BiOX and all these results demonstrate that the BiOCl nanoplates prepared by the present method are well crystallized with highly exposed {001} facets,[14,19,30] which supports the result of XRD analysis. EDS analysis (Fig. 4f) confirms the presence of Al, Bi, O, Cl and Br. The ratio of Cl and Br was ~4.1 which is in agreement with the XRD analysis. Quantitative EDS analysis was performed to calculate the relative amounts (in wt%) of $BiOCl_xBr_{1-x}$ with alumina, which is estimated to be ~78% and 22% for BiOClBr and alumina, respectively. The value is very close to the values expected from corresponding precursor materials.

The photocatalytic activity of these composite coatings with preferred orientation was estimated using RhB as a model pollutant under visible-light irradiation ($\lambda > 420$ nm). Fig. 5a demonstrates the sequential progress of the spectral changes during the photocatalytic decomposition of RhB by the coatings. Corresponding changes in RhB concentration (C/C_0) with irradiation time are presented in Fig. 5b. The direct photolysis test of RhB was performed over identical conditions and found that photolysis is negligible within the testing time. The adsorption–desorption equilibrium was achieved within 1 h by keeping at dark and it was observed that ~18% of RhB was adsorbed by the composite coating. Remarkably, ~78% of RhB was decomposed after 15 min of irradiation and almost complete degradation was achieved after 30 min of irradiation. The activity was almost doubled compared to the randomly oriented facets with similar compositions (ESI;† Fig. S6).[31] After the first cycle, the coated beaker reused for another 3 cycles. Interestingly, as shown in Fig. 5c, the activity maintains to be high even after 4 runs. Being the photocatalyst in the form of coatings, there is no trouble for the filtration of the catalyst after the completion of one cycle in contrast to the case of the powder material. This is very important for a successful industrial application.

In order to figure out the molecular mechanism of the photodegradation processes, trapping experiments were carried out for exploring the main photogenerated active oxidation species. This target has been accomplished by using common scavengers, *i.e.* benzoquinone (BQ), terephthalic acid (TA), potassium iodide (KI) for the superoxide radicals ($O_2^{\bullet-}$), hydroxyl radicals ($^{\bullet}OH$), and hole (h^+) species, respectively. It has been observed that the photodegradation of RhB is hardly inhibited when TA (a quencher of $^{\bullet}OH$) or KI (a quencher of h^+) was introduced to the photodecomposition tests, while a notable suppression has been realized in the presence of BQ (a quencher of $O_2^{\bullet-}$) (ESI;† Fig. S7). These results indicate that $O_2^{\bullet-}$ is the dominant active specie. Nevertheless, visible-light photocatalytic activity may also be originated from indirect dye photosensitization. It is possible that the RhB dye first absorbs the incident photon flux, and then injects the photoexcited electrons into the conduction band of the $BiOCl_xBr_{1-x}$ nanostructures, which later react with surface adsorbed molecular oxygen to generate the active species ($O_2^{\bullet-}$), and the subsequent reactions can lead to the degradation of RhB.

In summary, we have demonstrated a novel and unique method to fabricate $BiOCl_xBr_{1-x}$ solid solution coatings with

highly exposed {111} facets. The composite coatings showed better performances with respect to the similar films with random orientations of different facets. The proposed process has all the advanced benefits for industrial applications, *e.g.* easy to prepare, can be applied to different types of glass substrates, reusable for several cycles without any deterioration of their original activity. These important characteristics will make the material suitable for different environmental issues.

We acknowledge the financial support from the Israel Science Foundation (Grant No. 12/207).

Notes and references

1 J. Jiang, K. Zhao, X. Xiao and L. Zhang, *J. Am. Chem. Soc.*, 2012, **134**, 4473–4476.
2 G. Xi and J. Ye, *Chem. Commun.*, 2010, **46**, 1893–1895.
3 H. Xu, P. Reunchan, S. Ouyang, H. Tong, N. Umezawa, T. Kako and J. Ye, *Chem. Mater.*, 2013, **25**, 405–411.
4 Y. Bi, S. Ouyang, N. Umezawa, J. Cao and J. Ye, *J. Am. Chem. Soc.*, 2011, **133**, 6490–6492.
5 M. Leng, M. Liu, Y. Zhang, Z. Wang, C. Yu, X. Yang, H. Zhang and C. Wang, *J. Am. Chem. Soc.*, 2010, **132**, 17084–17087.
6 G. Liu, J. C. Yu, G. Q. Lu and H.-M. Cheng, *Chem. Commun.*, 2011, **47**, 6763–6783.
7 H. Gnayem and Y. Sasson, *ACS Catal.*, 2013, **3**, 186–191.
8 J. Wang and Y. Li, *Chem. Commun.*, 2003, 2320–2321.
9 J. Li, Y. Yu and L. Zhang, *Nanoscale*, 2014, **6**, 8473–8488.
10 J. Xiong, Z. Jiao, G. Lu, W. Ren, J. Ye and Y. Bi, *Chem. – Eur. J.*, 2013, **19**, 9472–9475.
11 S. Shenawi-Khalil, V. Uvarov, S. Fronton, I. Popov and Y. Sasson, *J. Phys. Chem. C*, 2012, **116**, 11004–11012.
12 J. Fu, Y. Tian, B. Chang, F. Xi and X. Dong, *J. Mater. Chem.*, 2012, **22**, 21159–21166.
13 H. Liu, W. Cao, Y. Su, Y. Wang and X. Wang, *Appl. Catal., B*, 2012, **111–112**, 271–279.
14 M. Guan, C. Xiao, J. Zhang, S. Fan, R. An, Q. Cheng, J. Xie, M. Zhou, B. Ye and Y. Xie, *J. Am. Chem. Soc.*, 2013, **135**, 10411–10417.
15 H. Li and L. Zhang, *Nanoscale*, 2014, **6**, 7805–7810.
16 D. Wu, B. Wang, W. Wang, T. An, G. Li, T. W. Ng, H. Y. Yip, C. Xiong, H. K. Lee and P. K. Wong, *J. Mater. Chem. A*, 2015, **3**, 15148–15155.
17 L. Ye, L. Zan, L. Tian, T. Peng and J. Zhang, *Chem. Commun.*, 2011, **47**, 6951–6953.
18 L. Sun, L. Xiang, X. Zhao, C.-J. Jia, J. Yang, Z. Jin, X. Cheng and W. Fan, *ACS Catal.*, 2015, **5**, 3540–3551.
19 L. Ye, L. Tian, T. Peng and L. Zan, *J. Mater. Chem.*, 2011, **21**, 12479–12484.
20 H. Li, J. Shang, Z. Ai and L. Zhang, *J. Am. Chem. Soc.*, 2015, **137**, 6393–6399.
21 H. Zhang, L. Liu and Z. Zhou, *RSC Adv.*, 2012, **2**, 9224–9229.
22 G. Liu, T. Wang, S. Ouyang, L. Liu, H. Jiang, Q. Yu, T. Kako and J. Ye, *J. Mater. Chem. A*, 2015, **3**, 8123–8132.
23 H. Gnayem and Y. Sasson, *J. Phys. Chem. C*, 2015, **119**, 19201–19209.
24 A. Dandapat, D. Jana and G. De, *ACS Appl. Mater. Interfaces*, 2009, **1**, 833–840.
25 A. Dandapat and G. De, *J. Mater. Chem.*, 2010, **20**, 3890–3894.
26 L. Ji, J. Lin, K. L. Tan and H. C. Zeng, *Chem. Mater.*, 2000, **12**, 931–939.
27 T. Xie, L. Xu, C. Liu, J. Yang and M. Wang, *Dalton Trans.*, 2014, **43**, 2211–2220.
28 M. Chen, X. Wang, Y. H. Yu, Z. L. Pei, X. D. Bai, C. Sun, R. F. Huang and L. S. Wen, *Appl. Surf. Sci.*, 2000, **158**, 134–140.
29 Z. Fu, T. Jiang, L. Zhang, B. Liu, D. Wang, L. Wang and T. Xie, *J. Mater. Chem. A*, 2014, **2**, 13705–13712.
30 X. Zhang, X.-B. Wang, L.-W. Wang, W.-K. Wang, L. L. Long, W.-W. Li and H.-Q. Yu, *ACS Appl. Mater. Interfaces*, 2014, **6**, 7766–7772.
31 H. Gnayem, A. Dandapat and Y. Sasson, *Chem. – Eur. J.*, 2015, DOI: 10.1002/chem.201503900.

